Korean J. Chem. Eng., 36(3), 385-392 (2019)
DOI: 10.1007/s11814-018-0219-1

pISSN: 0256-1115
eISSN: 1975-7220

Pd nanoparticles immobilized on TiO_2 nanotubes-functionalized ceramic membranes for flow-through catalysis

Jianfeng Miao‡, Xiaoyue Liu‡, Hong Jiang, Yefei Liu, and Rizhi Chen†

State Key Laboratory of Materials-Oriented Chemical Engineering, Nanjing Tech University, Nanjing 210009, P. R. China
(*Received 1 November 2018 • accepted 20 December 2018*)

Abstract−A high performance catalytic membrane was fabricated with Pd nanoparticles supported by TiO_2 nanotubes, where the TiO_2 nanotubes were synthesized on the ceramic membrane via a simple hydrothermal etching. A flow-through catalytic membrane reactor was developed for testing the catalytic properties in the *p*-nitrophenol reduction. The effect of etching time was investigated in detail and an optimal etching time was determined to be 16 h. The characterization results highlighted that the as-prepared bouquet-like TiO_2 nanotubes could significantly improve the loading amount and dispersity of Pd nanoparticles. The fabricated catalytic membrane exhibited considerably improved catalytic activity and stability, with a 100% conversion of *p*-nitrophenol and no loss in catalytic activity during five reaction cycles. The obtained activation energy was much lower than the values in literatures, implying that the *p*-nitrophenol reduction could take place more easily on our catalytic membranes compared to other catalysts.

Keywords: Catalytic Membrane, Pd Nanoparticles, Tio_2 Nanotubes, Ceramic Membranes, *p*-Nitrophenol Reduction

INTRODUCTION

Catalytic membrane reactors have attracted considerable attention owing to the distinctive ability to simultaneously carry out a chemical reaction and mass transfer into and out of the reaction zone [1-3]. Catalytic membrane reactors can be traced back to 1960s, proposed by Gryaznov for the first time [4]. Most of the early-stage research on catalytic membrane reactors focused on the gas phase reactions, where membranes (such as dense metal membranes) were used to remove the gases produced from the reaction mixture, breaking through thermodynamic equilibrium restriction, thereby achieving higher conversion of reactants or higher selectivity of desired products [5,6]. For example, Lin et al. [7] employed a defect-free palladium membrane reactor for an integrated production and purification process of hydrogen. In the steam reforming of methane, the reaction rate was significantly advanced with the assistance of a gas separation membrane module, and the conversion reached 45%, which was 15% higher than the thermodynamic equilibrium conversion.

With the development of catalytic membrane reactors, more efforts were made toward the liquid-solid and gas-liquid-solid multiphase reactions, and the function of membranes was further enriched [8-10]. The membrane can act as the carrier of catalytic active components or has catalytic performance itself [11]. Liu et al. [12] presented a new chiral catalytic membrane reactor which was constructed by immobilizing Mn (III) catalysts onto ceramic membranes. The results for the asymmetric epoxidation of styrene showed that the catalytic membrane reactor had more stable catalytic performance as compared to the homogeneous Mn (III) catalyst under the same reaction conditions. Additionally, the membrane catalyst could be reused directly without downstream separation.

In comparison with powder catalysts, catalytic membranes are capable of easily separating the catalysts from the reaction mixture, so it is propitious to realize the cyclic use of catalysts [13]. However, due to the limited available surface area for the access of reactants, catalytic membranes have internal deficiency [14]. Thus, a large number of membrane areas are required in terms of the limited reaction capacity. For example, when a catalytic membrane reactor was applied to partial hydrogenation of soybean oil, standard commercial treatment of 5-20 t of oil required 1,500-7,300 m^2 of membrane surface area [15], which would significantly increase the cost of industrial application. Consequently, improving the catalytic efficiency of a catalytic membrane is urgent, and has become a hot research topic.

To date, various approaches have been attempted to improve the catalytic performance of catalytic membranes, such as membrane modification, membrane configuration optimization and development of novel preparation methods [16-18]. Wang et al. [16] immobilized Pd/Fe nanoparticles in hydrophilically modified PVDF membranes for catalytic dechlorination of trichloroacetic acid. The modified PVDF membranes were able to decrease the aggregation of nanoparticles. The catalytic dechlorination rate with Pd/Fe-based hydrophilized PVDF membrane was 6.8-times greater than that with Pd/Fe-based unmodified PVDF membrane. Mahdavi et al. [17] developed a novel approach for the fabrication of catalytic polymeric membranes comprised of hierarchical nanostructures. Catalytic polymeric membranes were prepared by loading Pd decorated multi-wall carbon nanotubes (Pd-MWCNT) in polysulfone membranes. For selective oxidation of benzylalcohol, the resultant catalytic membrane exhibited better reactivity and reusability than the conventional catalytic membrane containing free Pd-MWCNT. Our

†To whom correspondence should be addressed.
E-mail: rizhichen@njtech.edu.cn
‡These authors equally contribute to this work.

group [18] successfully synthesized an efficient and reusable catalyst by depositing Pd nanoparticles on a hollow fiber ceramic membrane. As compared to tubular ceramic membrane, the fiber ceramic membrane could provide more surface area for the loading of palladium, thereby higher Pd content and catalytic activity. Very recently, we used TiO_2 nanorods to functionalize the ceramic membrane surface and then loaded Pd nanoparticles [19]. The modification with TiO_2 nanorods could increase the area, resulting in increased Pd loading and enhanced catalytic activity. Our previous work often directly put catalytic membranes into reactive systems [18,19]. In essence, these membranes serve as a porous support for incorporating active sites of catalysts rather than an integrative separation and reaction device.

In this contribution, a flow-through catalytic membrane reactor was designed, where the reactant solution was pumped through the membrane pores, in favor of access to active sites. TiO_2 nanotubes on ceramic membranes were fabricated via a simple in situ acid etching of TiO_2 nanorods in company with the deposition of Pd nanoparticles. The significant influence of the functionalization of TiO_2 nanotubes was investigated by characterizing the catalytic membranes with XRD, FESEM, HRTEM, ICP and XPS, and evaluating the catalytic properties with the *p*-nitrophenol reduction as the model reaction.

EXPERIMENTAL

1. Chemicals

Titanium butoxide (98.0%) and concentrated hydrochloric acid (36.5-38 wt%) were purchased from Shanghai Ling Feng chemical reagents Co., Ltd., China. Palladium acetate was obtained from Sinoplatinum Metals Co., Ltd., China. N-(*β*-aminoethyl)-*γ*-aminopropyl trimethoxy silane (AAPTS) was provided by Nanjing Capatue Chemical Co., Ltd., China. Other chemicals were of analytical grade and used as received without further purification. Sheet alumina ceramic membrane (3 μm in pore size, 3.2 cm in diameter and 2 mm in thickness, marked as CM) was obtained from Jiangsu Jiuwu Hi-Tech Co., Ltd., China.

2. Preparation of Catalytic Membranes

The preparation of catalytic membranes can be divided into three steps. First, bouquet-like TiO_2 nanorod arrays were prepared directly on CM substrates via a two-step hydrothermal method according to our previous work [19]. Subsequently, the in situ conversion of nanorods into nanotubes was conducted by immersing the obtained TiO_2 nanorods-modified CM in 40 mL of hydrochloric acid aqueous solution (the volume ratio of deionized water to concentrated hydrochloric acid was 1 : 1) at 150 °C for 8-20 h. After the synthesis of TiO_2 nanotubes-modified CM, the sample was extensively rinsed with deionized water for several times until it was neutral, and dried in an oven at 60 °C for 4 h (the boiling point of hydrochloric acid is 57 °C). Thus, the chlorine impurity on the sample might be completely removed. Finally, the TiO_2 nanotubes-modified CM was immersed in 50 mL of AAPTS dichloromethane solution (1 g/L) at 25 °C for 8 h. Then, the final catalytic membranes were synthesized by immersing the samples in a 0.05 mol/L Pd nanoparticle colloid [20] (50 mL) at 40 °C for 12 h. The colloid was synthesized by stirring the mixture (0.56 g of palladium acetate, 5.55 g of polyvinylpyrrolidone (PVP) and 50 mL of analytically pure ethanol) in a 250 mL beaker flask at 60 °C for 2 h.

The variation of the etching time in the hydrothermal etching process plays an important role in the synthesis of TiO_2 nanotubes and catalytic membranes. The as-prepared catalytic membranes with different etching time were named as Pd/TiO_2-CM-t (t refers to the etching time). In addition, for comparison, Pd loaded bare CMs were also fabricated under the same conditions and denoted as Pd/CM.

3. Characterization of Catalytic Membranes

The crystal structures of the TiO_2 nanotubes on CMs were analyzed by X-ray diffraction (XRD, MiniFlex-600). The data were recorded in the 2θ range from 10° to 80° with a scanning velocity of 10° per minute. The distribution of elemental Pd on the surface and the cross section of catalytic membranes was analyzed by energy-dispersive X-ray spectroscopy (EDS). The morphology of TiO_2 nanotubes-modified CMs as well as the immobilized Pd nanoparticles was characterized by the field emission scanning electron microscope (FESEM, Hitachi S-4800II) and the high-resolution transmission electron microscopy (HRTEM, JEM-2010). The Pd content of catalytic membranes was evaluated via inductively coupled plasma emission spectroscopy (ICP, Optima 2000 DV). Before ICP analysis, catalytic membranes were immersed in 20 mL 10% (v/v) nitric acid (65-68 wt%) aqueous solution at 60 °C for 2 h. X-ray photoelectron spectrometry (XPS, Thermo ESCALAB 250) was applied to investigate the surface composition and chemical states of all elements. The binding energy of the C 1s main peak was set at 284.8 eV for charge correction.

4. Catalytic Performance Evaluation

The reduction of *p*-nitrophenol (Scheme 1) was chosen for determining the catalytic activity and stability of the produced catalytic membranes. During the reaction, Pd nanoparticles accepted electrons from BH_4^- ions and conveyed them to *p*-nitrophenol molecules, promoting the reduction [21,22]. First, *p*-nitrophenol and $NaBH_4$ were absorbed on the surface of Pd nanoparticles, and BH_4^- ions transferred H species to the surface of Pd nanoparticles. Second, H species transferred from Pd nanoparticles to *p*-nitrophenol. Finally, the reduction performed step by step, and then *p*-aminophenol was formed.

Catalytic performance test was carried out in a flow-through catalytic membrane reactor as presented in Fig. 1. The reactor was built with a membrane module, a storage tank and a peristaltic pump. A water bath was used to keep the reaction temperature constant. At the beginning of each experiment, 60 mL of reaction mixture (10 mL of ethanol and 50 mL of water) containing 0.45 g of *p*-nitrophenol and 0.65 g of $NaBH_4$ (molar ratio 1 : 5.3) was loaded into the storage tank. The membrane module and storage tank were put in the water bath for the sake of maintaining the reactant solution at 30 °C. The concentration of *p*-nitrophenol was measured

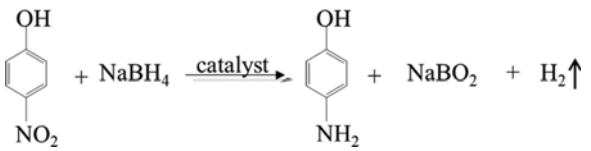

Scheme 1. Reduction of *p*-nitrophenol to *p*-aminophenol with $NaBH_4$.

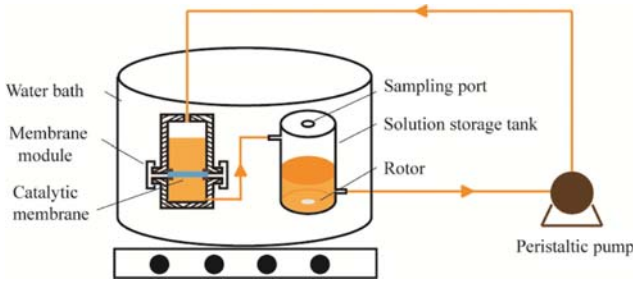

Fig. 1. Experimental setup of flow-through catalytic membrane reactor.

before recycling experiment, and it was found that no *p*-nitrophenol was converted, confirming that the reaction would not occur without catalyst. The reaction was started when the reactant solution was introduced into the membrane module by a peristaltic pump (flow rate 45 mL/min). The reactor was operated in a recycle mode under a filtration pressure of 0.25 bar. During the reaction, the mixture was pumped through the membrane pores and contacted with catalytic active component, and then back to the tank. For product analysis, small amounts of the solution were taken from the sampling port of the tank every 5 minutes, and the composition was analyzed by high performance liquid chromatography (HPLC, Agilent 1200 series).

5. Establishment of Kinetics Model

The power function dynamic equation can reflect the influence of the component concentration and the reaction temperature on the reaction rate, and can simulate the experimental data more accurately [23]. So the reaction rate of the *p*-nitrophenol reduction can be described as the following equations:

$$r_A = -\left(\frac{dC_A}{d_t}\right) = kC_A^a C_B^b \quad (1)$$

$$k = k_0 \exp\left(-\left(\frac{E_a}{RT}\right)\right) \quad (2)$$

where r is the reaction rate ($mol \cdot L^{-1} \cdot min^{-1}$), k is the reaction rate constant, C_A and C_B are the concentrations of *p*-nitrophenol and $NaBH_4$ ($mol \cdot L^{-1}$), a and b are the corresponding reaction orders, E_a is the activation energy ($kJ \cdot mol^{-1}$), T is the reaction temperature (K), k_0 is the pre-exponential factor, and R is the gas constant ($kJ \cdot mol^{-1} \cdot K^{-1}$).

The initial rate method [24] was adopted to examine the initial reaction rate of *p*-nitrophenol. Effects of various reaction conditions on the reaction rate of *p*-nitrophenol were investigated, and parameters of kinetic model were obtained through changing a series of single factors such as the rotate rate of peristaltic pump, *p*-nitrophenol concentration, $NaBH_4$ concentration and reaction temperature.

RESULTS AND DISCUSSION

1. Synthesis and Characterization of Catalytic Membranes

The diffraction peaks in the XRD patterns of catalytic membranes are mainly attributed to the alumina ceramic membrane substrate (Fig. S1). Compared to Pd/CM (Fig. S1(a)), in Pd/TiO_2-CM (Fig. S1(b)-(f)), three new diffraction peaks are observed at 2θ= 27.4° (major), 41.2° and 54.3°, which corresponds to the characteristic diffractions of the (110), (111) and (211) planes of rutile TiO_2 (JCPDS No. 21-1276), respectively [25,26]. No peak corresponding to the (001) crystal facet is observed, which can be explained as follows. In this work, TiO_2 nanotubes grew vertically on the ceramic membrane (Fig. 2), and the (001) crystal facet with high energy was preferentially etched. On the other hand, the diffraction peaks of the ceramic membrane are very strong (Fig. S1). The results indicate the successful functionalization of TiO_2 nanotubes on the ceramic membrane. The etching time has no obvious influence on the intensity, which may be correlation with the surface energies of different facets of TiO_2 nanorods. The surface energy of the rutile TiO_2 nanorods follows the sequence of (110)<(100)<(101)<(001), and the facet with higher surface energy diminishes faster for the minimization of the total surface energy [25,27]. Therefore, the top (001) crystal facet with high energy is etched faster than the (110) facet. Thus, the converting of TiO_2 nanorods to nanotubes by a hydrothermal method can selectively etch the core and

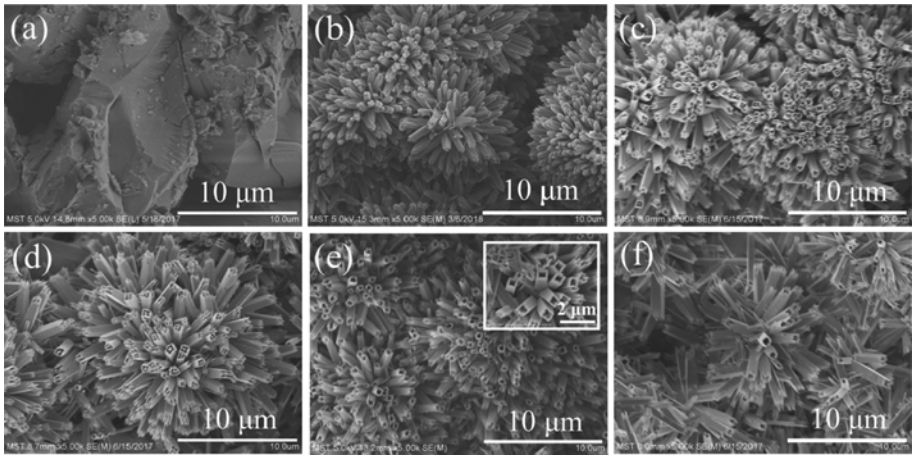

Fig. 2. Surface FESEM images of (a) Pd/CM, (b) Pd/TiO_2-CM-0, (c) Pd/TiO_2-CM-8, (d) Pd/TiO_2-CM-12, (e) Pd/TiO_2-CM-16, (f) Pd/TiO_2-CM-20.

remain the sidewall of (110) face, thereby no significant change in the major diffraction peak of TiO_2 nanotubes under different etching time. There are no obvious characteristic diffraction peaks of metal Pd in the XRD patterns. Two factors may cause this result: one is that the size of Pd nanoparticles is too small, the other is the immobilized Pd is highly dispersed on the CM [28].

Fig. 2 shows the morphology of TiO_2 nanotubes on CMs with different etching time. The bouquet-like TiO_2 nanorods are fully covered on the surface of CM, without large-area domains of CM exposed (Fig. 2(a) and (b)). After acid etching treatment under hydrothermal conditions for 8, 12, 16 h (Fig. 2(c), (d) and (e)), the TiO_2 nanorods are gradually transformed into hollow TiO_2 nanotubes. It confirms that the corrosion rate along the core facet of nanorods is faster than the inert sidewall [25]. As shown in the insert of Fig. 2(e), the square columnar TiO_2 nanotubes have smooth side walls, and tube width, wall thickness and tube length are about 500-800 nm, 50 nm and 4 μm, respectively. While the etching time is increased to 20 h (Fig. 2(f)), the side walls of TiO_2 nanotubes are corroded, and so the nanotubes are partly damaged. Similar experimental phenomena were found by Lv et al. [29] Herein, a suitable etching time is 16 h for the formation of TiO_2 nanotubes on the ceramic membranes.

To confirm the successful loading of Pd on CM and investigate the influence of TiO_2 nanotubes on the Pd loading, SEM-EDS mapping was performed on two typical samples: Pd/CM and Pd/TiO_2-CM-16. In Fig. 3, element Pd is found to be present on the surface of bare CM, but only in a small amount. However, the distribution of Pd on the surface of Pd/TiO_2-CM-16 is rather intensive and uniform. Fig. 4 shows the Pd element distribution on the cross section of Pd/CM and illustrates smaller amount of Pd compared to Pd/TiO_2-CM-16, meaning that more Pd is loaded in the pores of the TiO_2 nanotubes-modified CM. The results highlight that Pd nanoparticles can be successfully deposited on the membrane surface and inside the pores, and TiO_2 nanotubes can significantly improve the loading amount and dispersity of Pd on the CM.

ICP analysis was carried out to evaluate the actual loading amounts of the six catalytic membranes. The actual loading amounts of Pd on CM, TiO_2-CM-0, TiO_2-CM-8, TiO_2-CM-12, TiO_2-CM-16 and TiO_2-CM-20 are 0.123, 0.142, 0.186, 0.187, 0.196 and 0.183 mg/cm^2 respectively. It is immediately apparent that the etching time strongly affects the Pd loading, the Pd/TiO_2-CM-16 has the highest content of Pd, and the trend coincides with the FESEM results (Fig. 2). This indicates that the nanotube structure can effectively enlarge the surface area of CM and provide more area for the loading of Pd, thereby higher Pd content.

Fig. 5 provides the representative TEM images and the Pd particle size distribution of the power taken from Pd/CM and Pd/TiO_2-CM-16. The Pd particles are uniformly distributed on the TiO_2 nanotubes-modified CM and exhibit a narrow size distribution

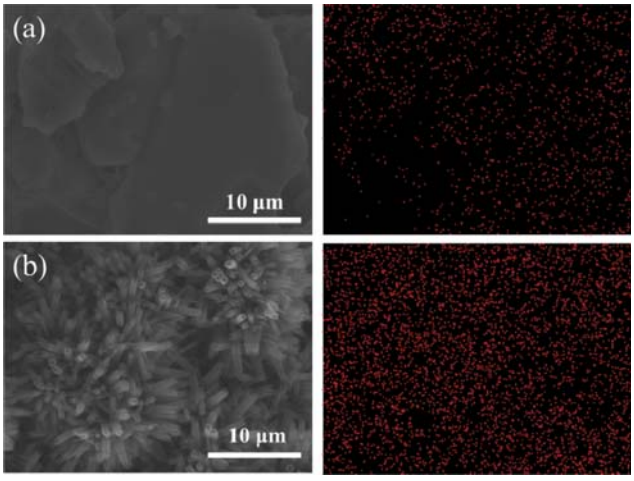

Fig. 3. SEM pictures and EDS analysis of the distribution of elemental Pd on the surface of (a) Pd/CM and (b) Pd/TiO_2-CM-16.

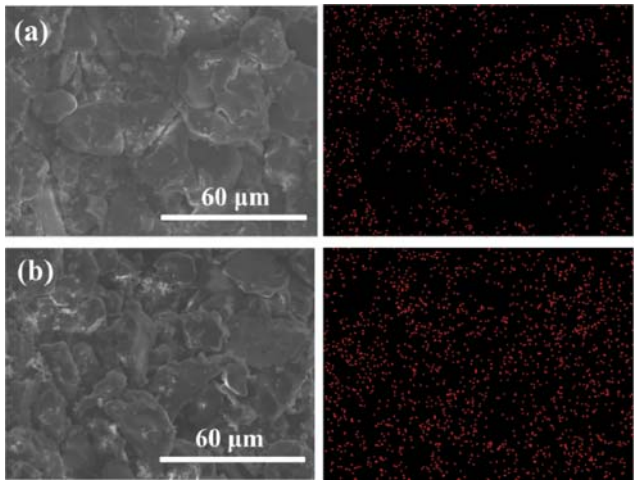

Fig. 4. SEM pictures and EDS analysis of the distribution of elemental Pd on the cross section of (a) Pd/CM and (b) Pd/TiO_2-CM-16.

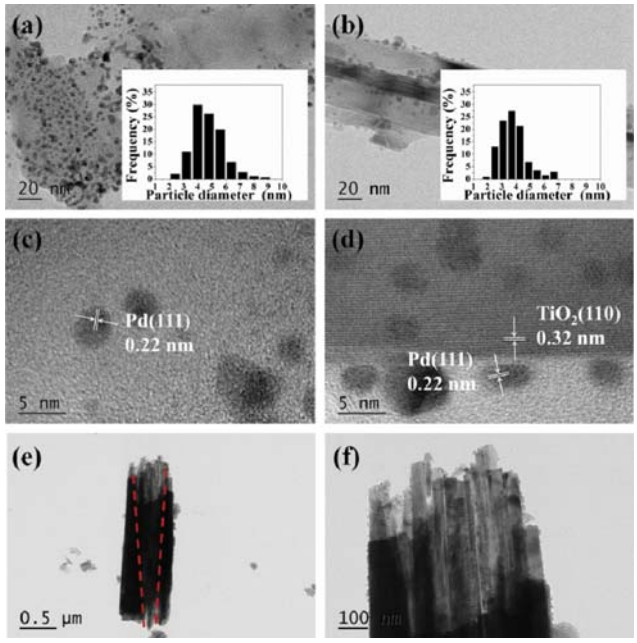

Fig. 5. TEM images of the powder taken from (a), (c) Pd/CM, (b), (d), (e), (f) Pd/TiO_2-CM-16.

with an average particle size of 3.8 nm (Fig. 5(b)). In contrast, Pd/CM (Fig. 5(a)) has a larger average metal particle size (4.7 nm), implying that TiO_2 nanotubes grown on the CM are beneficial to obtain Pd nanoparticles with better dispersity and smaller size. As presented in Section 2.2, the catalytic membranes were synthesized by immersing the CMs in a Pd nanoparticle colloid at 40 °C for 12 h. Thus, during the synthesis of catalytic membranes, Pd nanoparticles may have aggregated [30]. TiO_2 nanotubes on the CM can provide more surface area for the loading of Pd nanoparticles, and roughen the surface of the CM to play the role of anchoring. Therefore, in the loading process, the TiO_2 nanotubes-modified CM might effectively prevent the agglomeration of Pd nanoparticles and improve their dispersion. Fig. 5(c) and (d) gives high-magnification views of the power taken from the two catalytic membranes. Particles in two images both display a lattice spacing of 0.22 nm that belongs to the (111) plane of the Pd phase [31], further confirming the successful loading of Pd nanoparticles. Fig. 5(d) shows a lattice spacing of 0.32 nm that corresponds to the (110) plane of rutile TiO_2 [29], consistent with the XRD characterization (Fig. S1). More interestingly, the TiO_2 nanotubes have a V-shaped hollow structure and a rectangular cross-section, which is specially shown in Fig. 5(e). The formation of V-shaped hollow structure might be attributed to the decreasing concentration gradient of hydrochloric acid along the etching direction and the further erosion of the exposed sidewall [32]. Furthermore, it can be clearly observed from Fig. 5(f) that the Pd nanoparticles can be immobilized on the inner and outer surfaces of TiO_2 nanotube, which may be responsible for higher Pd content in Pd/TiO_2-CM compared to Pd/CM.

Peaks corresponding to Al, O, Si, N and Pd are clearly found in Pd/CM from the XPS spectrum (Fig. S2). The Al and O are from CM, and the other three elements should be from the AAPTS and Pd nanoparticles anchored on CM, verifying the successful modification of CM with AAPTS and the subsequent deposition of Pd nanoparticles as presented in the Experimental section, in good agreement with our previous work [33]. Note that a new Ti 2p peak appears in the spectrum of Pd/TiO_2-CM-16 compared to Pd/CM, confirming the formation of TiO_2 nanotubes on the CM (Figs. S1, S2 and S5). Pd atomic contents of Pd/CM and Pd/TiO_2-CM-16 are 1.05% and 1.46% respectively, further confirming that the TiO_2 nanotubes can promote the amount of Pd loaded on the CM (Figs. 3 and 4). Two Pd species can be observed for the two catalytic membranes (Fig. S3). The peaks detected at 335.4 and 340.5 eV can be attributed to zero-valent Pd (Pd^0), and the ones at 337.1 eV and 342.6 eV are assigned to divalent Pd (Pd^{2+}) [34]. Pd/CM and Pd/TiO_2-CM-16 almost have the same ratio of Pd^0. However, combined with the total content of surface Pd atoms, Pd/TiO_2-CM-16 has a higher loading amount of Pd^0, which is beneficial for the increase in catalytic activity as discussed below.

2. Catalytic Performance Evaluation

Catalytic reduction of *p*-nitrophenol was performed to investigate the effect of the functionalization with TiO_2 nanotubes on the catalytic efficiency of catalytic membrane. Fig. 6 highlights that the functionalization with TiO_2 nanotubes can significantly enhance the catalytic activity. For example, for Pd/TiO_2-CM-16, the conversion of *p*-nitrophenol can reach 57% in only 5 minutes and complete reduction within 60 minutes. In contrast, with respect to Pd/CM, only 31% of conversion at 5 minutes and 98% of conversion at 60 minutes are achieved. Together with the foregoing characterization results, we can conclude that the functionalization of CM with TiO_2 nanotubes can provide more surface area for the loading of Pd, and improve the loading amount and dispersity of Pd, thereby increasing catalytically active sites and enhanced catalytic activity.

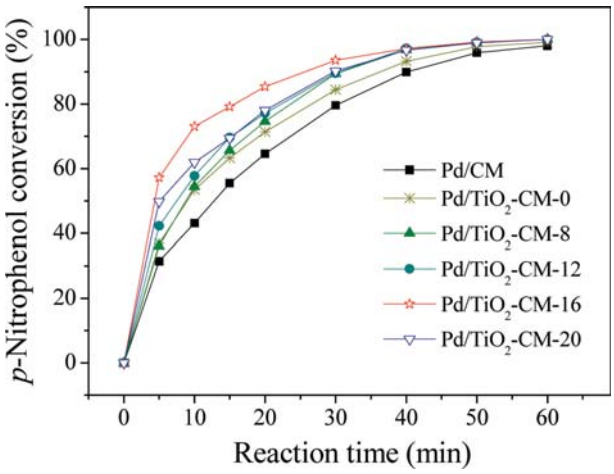

Fig. 6. Reaction profile of catalytic reduction of *p*-nitrophenol over different catalytic membranes.

The catalytic activity of Pd/TiO_2-CM strongly depends on the etching time of TiO_2 nanorods. With increasing etching time, its catalytic activity first increases, reaches the highest at an etching time of 16 h, and then is reduced. Combined with the ICP results, the catalytic activity of Pd/TiO_2-CM cannot match well with the Pd loading. For instance, the content of Pd in Pd/TiO_2-CM-20 is less than those of Pd/TiO_2-CM-8 and Pd/TiO_2-CM-12, but its activity is higher. This phenomenon may be caused by the larger opening TiO_2 nanotube structure in Pd/TiO_2-CM-20 (Fig. 2), which is beneficial for the transfer of reactants to the surface of Pd nanoparticles (Fig. 5), corresponding to higher reactivity. Thus, it is reasonable to presume that suitable etching time of TiO_2 nanorods is highly important, which determines the Pd loading and the opening structure of nanotubes, thereby affecting the catalytic efficiency.

While we have demonstrated that Pd/TiO_2-CM-16 has superior catalytic activity, it is highly important to examine its recyclability over multiple reaction cycles from the point view of practical application. For comparison, the reusability of Pd-CM was also evaluated. In detail, after the reaction, the catalytic membrane was recovered simply by immersing in ethanol for 1 h, and then the recovered catalytic membrane was reused in the next run. The ethanol solution was analyzed by HPLC, and the results suggest that a small amount of *p*-aminophenol was adsorbed in the pores and nanotubes of the catalytic membrane during the reaction. Interestingly, for Pd/TiO_2-CM-16, the catalytic activity can almost be maintained even after five recycles (Fig. 7(b)), indicating Pd/TiO_2-CM-16 can preserve high catalytic activity toward *p*-nitrophenol reduction. Similar trend can be found with respect to Pd/CM, with only 3% deactivation. The results demonstrate that the as-prepared catalytic membranes have superior catalytic stability in the reduction

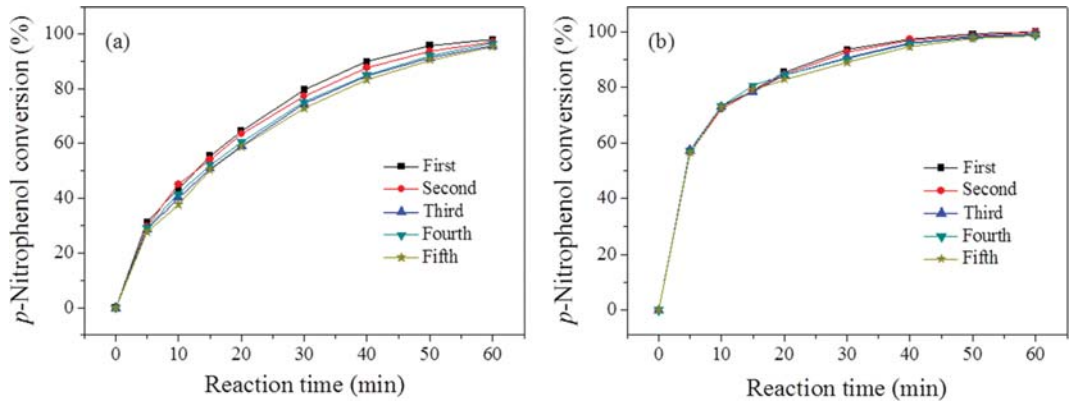

Fig. 7. Change of catalytic activity with reaction cycle: (a) Pd/CM and (b) Pd/TiO_2-CM-16.

of *p*-nitrophenol to *p*-aminophenol, owing to the chemical binding of Pd nanoparticles on the membranes through the bridging function of AAPTS [19,20].

To investigate the evolution of catalytic membranes after completion of the recycling reaction, the recovered catalytic membranes were characterized by FESEM, EDS and TEM. The morphologies of the recovered Pd/CM and Pd/TiO_2-CM-16 are similar to the fresh samples (Fig. S4), indicating that the ceramic membrane and TiO_2 nanotubes can maintain their structures during the reaction cycles. Furthermore, on the basis of the results of the EDS analysis (Fig. S5), a large number of Pd nanoparticles are still evenly distributed on the membrane surface, similar to the fresh ones (Fig. 3). Compared to the fresh samples (Fig. 5), slight increase in Pd particle size after five catalytic reaction cycles is observed (Fig. S6), which may be responsible for the slight deactivation (Fig. 7). Metal nanoparticles with high surface energy tend to aggregate during reactions, resulting in the deactivation of catalysts [30]. The results further confirm the superior reusability of the as-prepared catalytic membranes.

3. Kinetic Study

The developed Pd/TiO_2-CM-16 exhibits superior catalytic performance in the reduction of *p*-nitrophenol to *p*-aminophenol (Figs. 6 and 7). To further evaluate its catalytic behavior, the kinetics of the reduction of *p*-nitrophenol over Pd/TiO_2-CM-16 was studied.

Catalytic reduction of *p*-nitrophenol to *p*-aminophenol on the

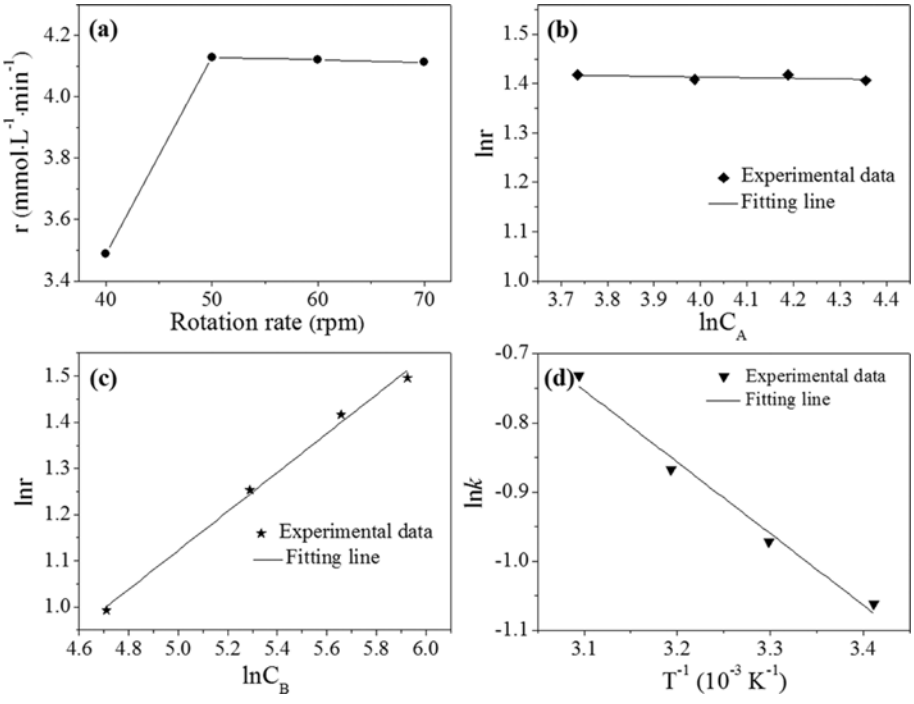

Fig. 8. Dependence of initial reaction rate on the reaction conditions: (a) Rotation rate of peristaltic pump, (b) *p*-nitrophenol concentration, (c) $NaBH_4$ concentration and (d) reaction temperature (elementary reaction conditions: *p*-nitrophenol concentration 54 mmol/L, $NaBH_4$ concentration 286 mmol/L, reaction temperature 30 °C, rotation rate 50 rpm).

catalytic membrane is a typical liquid-solid two-phase reaction. The reactants need to flow through the membrane pores and react on the surface of the Pd nanoparticles. Therefore, the reaction rate may be affected by mass transfer resistance. The Pd nanoparticles in Pd/TiO_2-CM-16 have an average particle size of about 3.8 nm (Fig. 5(b)). The modified Thiele modulus is on the order of 10^{-11} to 10^{-9}, much smaller than$|n|^{-1}$ (n is the total reaction order). Therefore, there is no internal diffusion during the reaction according to the Mears criterion [35]. Generally, the external mass transfer resistance is directly related to the flow rate of the reaction solution. In this work, in order to investigate the effect of the external diffusion resistance, the initial reaction rate of *p*-nitrophenol was investigated under different rotation rates of peristaltic pump (40-70 rpm, in proportion of the flow rate), while the other reaction conditions were kept constant. As shown in Fig. 8(a), with increasing rotation rate, the initial reaction rate of *p*-nitrophenol first increases and then remains almost steady when the rotation rate surpasses 50 rpm, suggesting that the influence of the external diffusion on the reaction has been basically eliminated.

Interestingly, the initial reaction rate is independent of the increased *p*-nitrophenol concentration within the experimental range. The plot of $\ln C_A$ against $\ln r$ is a horizontal line, as shown in Fig. 8(b). The results indicate that the order of the reaction to *p*-nitrophenol is 0. Fig. 8(c) shows that $\ln r$ depends linearly on $\ln C_B$ and the slope of linear equation is 0.42, manifesting the reaction order with respect to $NaBH_4$ is 0.42. So the total reaction order of the reaction is 0.42, which is a significant difference from the reported first-order reaction [36-38]. The molar ratio of $NaBH_4$ to *p*-nitrophenol may be the cause of this difference. In our work, the molar ratio is just 5.3, which is much smaller than the reported value (>100).

The dependence of the reaction rate constant k on the reaction temperature is described by the Arrhenius Eq. (2). The rate constant k of the reaction within a temperature range of 20 to 50 °C is calculated and summarized in Fig. 8(d). The plot of lnk vs 1/T can be represented by a straight line. So the activation energy is 8.61 kJ/mol and the pre-exponential factor is 11.67 $mmol^{0.58}\cdot L^{-0.58}\cdot min^{-1}$ on the basis of the slope and intercept of line. The calculated activation energy is much lower than those of the literature (36.72 kJ/mol [39] and 20-70 kJ/mol [40]), implying that the *p*-nitrophenol reduction can take place more easily on Pd/TiO_2-CM-16 compared to other catalysts. Smaller Pd nanoparticles, which can provide more active sites and fast mass transfer ascribed to flow-through model of catalytic membrane reactor, may be the causes of lower activation energy. For example, Pd nanoparticles in the PVDF composite membranes prepared by Wang et al. [39] were about 15-25 nm in size, which was much larger than Pd nanoparticles (Fig. 5(b), 3.8 nm) in our research.

CONCLUSIONS

TiO_2 nanotubes-functionalized ceramic membranes were successfully fabricated and employed as the support of Pd nanoparticles to synthesize highly efficient catalytic membranes. Pd nanoparticles with smaller size and higher content could be homogeneously precipitated on functionalized ceramic membranes. The produced catalytic membrane showed remarkable catalytic efficiency for *p*-nitrophenol reduction with $NaBH_4$ in the developed flow-through catalytic membrane reactor, and there was no distinct decrease in catalytic activity after fifth cycle. The use of TiO_2 nanotubes to functionalize ceramic membranes appears to be a very promising approach for the fabrication of environmental friendly catalysts with high activity and no additional separation processes.

ACKNOWLEDGEMENTS

The financial support from the National Natural Science Foundation (21776127, 91534110), the Jiangsu Province Natural Science Foundation for Distinguished Young Scholars (BK20150044) and the Jiangsu Province Natural Science Foundation (BK20160978) of China is gratefully acknowledged.

SUPPORTING INFORMATION

Additional information as noted in the text. This information is available via the Internet at http://www.springer.com/chemistry/journal/11814.

REFERENCES

1. N. Kageyama, P. Hacarlioglu, A. Takagaki, R. Kikuchi and S. T. Oyama, *Sep. Purif. Technol.*, **185**, 175 (2017).
2. K. R. Hwang, S. K. Ihm and J. Park, *Korean J. Chem. Eng.*, **27**, 816 (2010).
3. C. H. Kim, J. Y. Han, H. Lim, D. W. Kim and S. K. Ryi, *Korean J. Chem. Eng.*, **34**, 1260 (2017).
4. V. M. Gryaznov, *Russ. Chem. Rev.*, **32**, 188 (1963).
5. L. Meng and T. Tsuru, *Catal. Today*, **268**, 3 (2016).
6. J. S. Choi, I. K. Song and W. Y. Lee, *Korean J. Chem. Eng.*, **17,** 280 (2000).
7. Y. M. Lin, G. L. Lee and M. H. Rei, *Catal. Today*, **44**, 343 (1998).
8. M. Vospernik, A. Pintar, G. Berci and J. Levec, *Catal. Today*, **79-80**, 169 (2003).
9. M. Liu, X. Zhu, R. Chen, Q. Liao, H. Feng and L. Li, *Chem. Eng. J.*, **301**, 35 (2016).
10. Z. H. Zhao, G. H. Tong and X. Y. Tan, *J. Chem. Technol. Biotechnol.*, **91**, 2298 (2016).
11. N. Diban, A. T. Aguayo, J. Bilbao, A. Urtiaga and I. Ortiz, *Ind. Eng. Chem. Res.*, **52**, 10342 (2013).
12. M. Liu, Z. P. Zhao, K. C. Chen and W. F. Liu, *Catal. Commun.*, **64**, 70 (2015).
13. R. L. Huang, H. X. Zhu, R. X. Su, W. Qi and Z. M. He, *Environ. Sci. Technol.*, **50**, 11263 (2016).
14. J. N. Armor, *J. Membr. Sci.*, **147**, 217 (1998).
15. M. D. Wales, L. B. Joos, W. A. Traylor, P. Pfrommb and M. Rezac, *Catal. Today*, **268**, 12 (2016).
16. X. Y. Wang, J. C. Yang, M. P. Zhu and F. Li, *J. Taiwan Inst. Chem. E.*, **44**, 386 (2013).
17. H. Mahdavi, A. Rahimi and T. Shahalizade, *J. Polym. Res.*, **23**, 1 (2016).
18. R. Z. Chen, Y. G. Jiang, W. H. Xing and W. Q. Jin, *Ind. Eng. Chem. Res.*, **52**, 5002 (2013).

19. S. Zhang, H. Jiang, Y. F. Liu and R. Z. Chen, *Can. J. Chem. Eng.*, **95**, 2374 (2017).
20. Y. Du and R. Z. Chen, *Korean J. Chem. Eng.*, **32**, 1759 (2015).
21. L. G. Dou and H. Zhang, *J. Mater. Chem. A.*, **4**, 18990 (2016).
22. A. Shukla, R. K. Singha, T. Sasaki and R. Bal, *Green Chem.*, **17**, 785 (2015).
23. M. Afrand, D. Toghraie and B. Ruhani, *Exp. Therm Fluid Sci.*, **77**, 38 (2016).
24. M. Boron, A. Corma, F. Illas, J. Radill, T. Ródenas and M. J. Sabater, *J. Catal.*, **278**, 50 (2011).
25. H. Huang, L. Pan, C. K. Lim, H. Gong, J. Guo, M. S. Tse and O. K. Tan, *Small*, **9**, 3153 (2013).
26. D. Li, X. W. Cheng, X. J. Yu and Z. P. Xing, *Chem. Eng. J.*, **279**, 994 (2015).
27. R. S. Zeng, K. Li, X. Sheng, L. P. Chen, H. J. Zhang and X. J. Feng, *Chem. Commun.*, **52**, 4045 (2016).
28. J. B. Zhong, Y. Lu, W. D. Jiang, Q. M. Meng, X. Y. He, J. Z. Li and Y. Q. Chen, *J. Hazard. Mater.*, **168**, 1632 (2009).
29. M. Q. Lv, D. J. Zheng, M. D. Ye, L. Sun, J. Xiao, W. X. Guo and C. J. Lin, *Nanoscale*, **4**, 5872 (2012).
30. M. Yurderi, A. Bulut, M. Zahmakiran, M. Gülcan and S. Özkar, *Appl. Catal. B: Environ.*, **160**, 534 (2014).
31. A. Mansouri and N. Semagina, *Appl. Catal. A*, **543**, 43 (2017).
32. L. Liu, J. S. Qian, B. Li, Y. M. Cui, X. F. Zhou, X. F. Guo and W. P. Ding, *Res. Chem. Intermed.*, **46**, 1569 (2010).
33. R. Z. Chen, Y. G. Jiang, W. H. Xing and W. Q. Jin, *Ind. Eng. Chem. Res.*, **50**, 4405 (2011).
34. C. Ao, P. F. Tian, L. Ouyang, G. J. Da, X. Y. Xu, J. Xu and Y. F. Han, *Catal. Sci. Technol.*, **6**, 5060 (2016).
35. G. W. Zhan, Y. L. Hong, F. F. Lu, A. R. Ibrahim, M. M. Du, D. H. Sun, J. L. Huang, Q. B. Li and J. Li, *J. Mol. Catal. A: Chem.*, **366**, 215 (2013).
36. V. K. Gupta, N. Atar, M. L. Yola, Z. Ustundag and L. Uzun, *Water Res.*, **48**, 210 (2014).
37. Y. C. Chang and D. H. Chen, *J. Hazard. Mater.*, **165**, 664 (2009).
38. J. Feng, L. Su, Y. H. Ma, C. L. Ren, Q. Guo and X. G. Chen, *Chem. Eng. J.*, **221**, 16 (2013).
39. Z. Y. Wang, X. Chen, K. Li, S. Y. Bi, C. L. Wu and L. Chen, *J. Membr. Sci.*, **496**, 95 (2015).
40. S. Y. Bi, K. Li, X. Chen, W. G. Fu, L. Chen, H. Y. Sheng and Q. Yang, *Polym. Compos.*, **35**, 2251 (2015).

Supporting Information

Pd nanoparticles immobilized on TiO_2 nanotubes-functionalized ceramic membranes for flow-through catalysis

Jianfeng Miao[‡], Xiaoyue Liu[‡], Hong Jiang, Yefei Liu, and Rizhi Chen[†]

State Key Laboratory of Materials-Oriented Chemical Engineering, Nanjing Tech University, Nanjing 210009, P. R. China
(*Received 1 November 2018 • accepted 20 December 2018*)

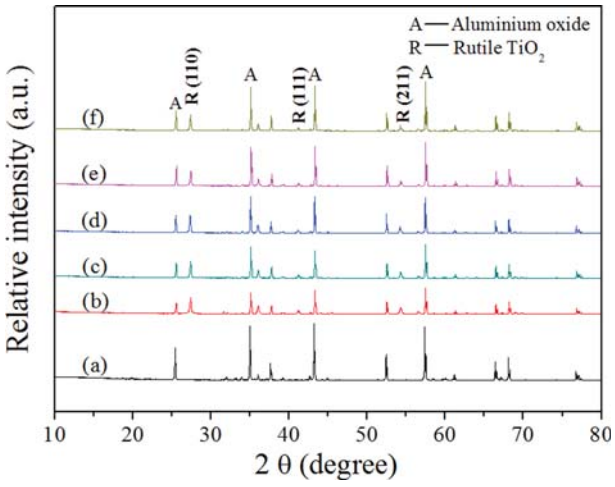

Fig. S1. XRD patterns of (a) Pd/CM, (b) Pd/TiO_2-CM-0, (c) Pd/TiO_2-CM-8, (d) Pd/TiO_2-CM-12, (e) Pd/TiO_2-CM-16, (f) Pd/TiO_2-CM-20.

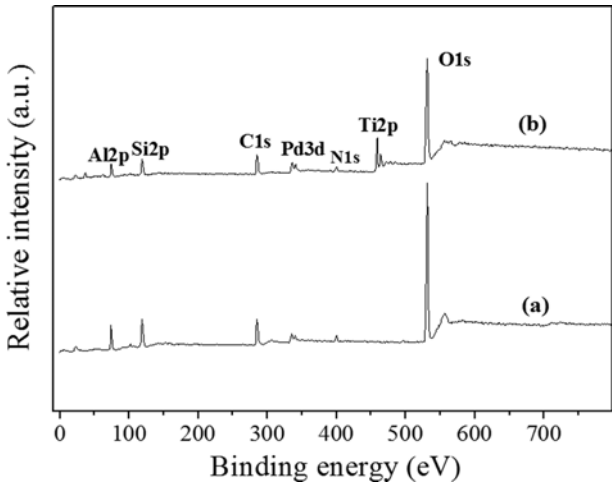

Fig. S2. XPS survey spectra of the powder taken from (a) Pd/CM, (b) Pd/TiO_2-CM-16.

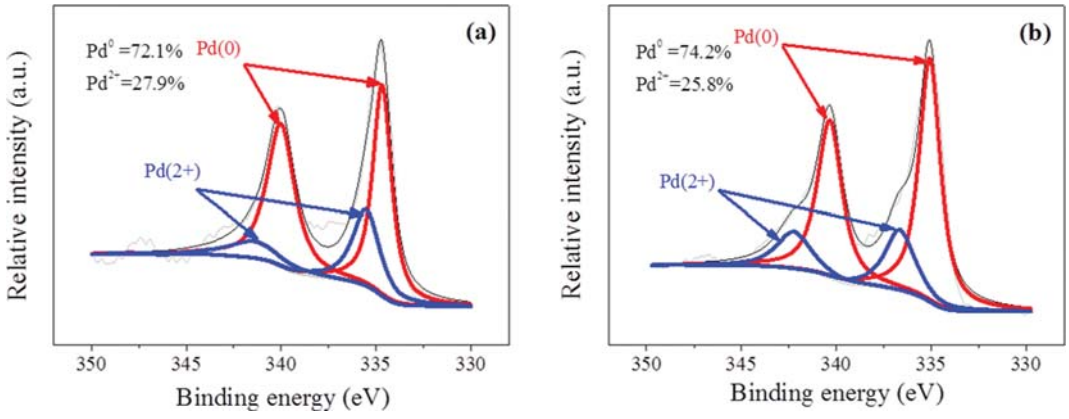

Fig. S3. Pd 3d XPS spectra of the powder taken from (a) Pd/CM, (b) Pd/TiO_2-CM-16.

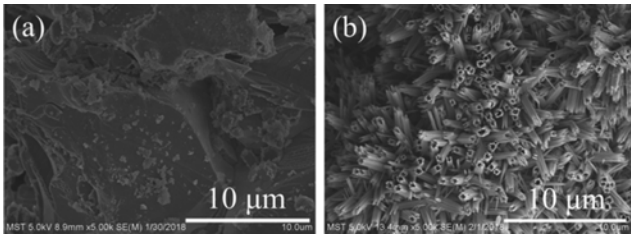

Fig. S4. Surface FESEM images of (a) Pd/CM and (b) Pd/TiO_2-CM-16 after fifth cycle.

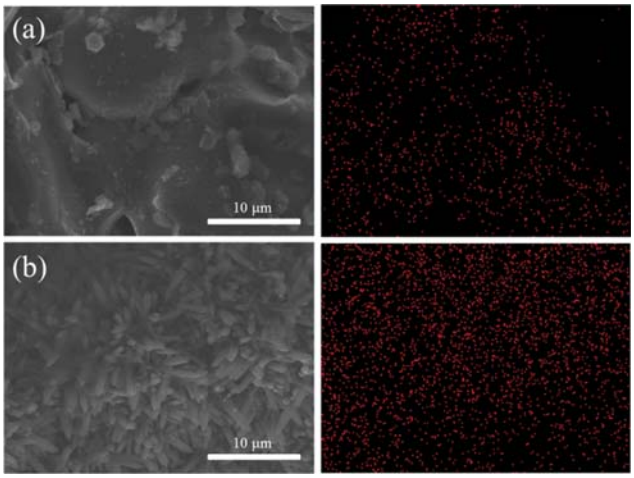

Fig. S5. EDS analysis of the surface of (a) Pd/CM and (b) Pd/TiO_2-CM-16 after fifth cycle.

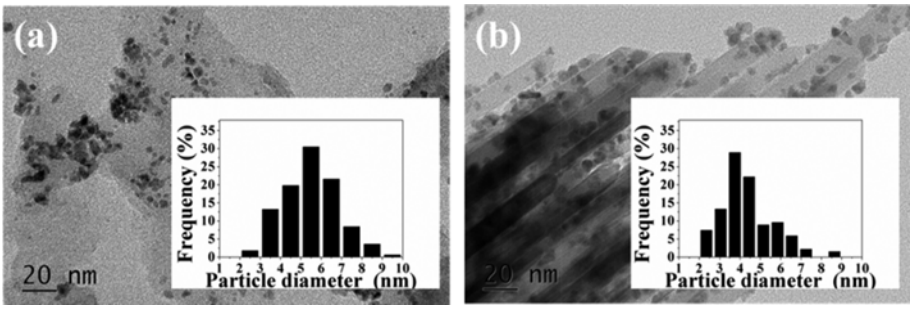

Fig. S6. TEM images of the powder taken from (a) Pd/CM and (b)Pd/TiO_2-CM-16 after fifth cycle.